Non-Uniform Global Demagnetization Detection in Interior PMSMs Using Search Coils

Marcos Orviz
Dept of Elect. Computer & System Engineering
University of Oviedo
Gijón, 33204, Spain
orvizmarcos@uniovi.es

David Reigosa
Dept of Elect. Computer & System Engineering
University of Oviedo
Gijón, 33204, Spain
diazdavid@uniovi.es

Jigyun Jeong
Department of Electrical Engineering
Korea University
Seoul, Korea
jjg0402@korea.ac.kr

Hyeon-Jun Lee
Department of Electrical Engineering
Korea University
Seoul, Korea
lhjoon14@gmail.com

Sang Bin Lee
Department of Electrical Engineering
Korea University
Seoul, Korea
sangbinlee@korea.ac.kr

Fernando Briz
Dept of Elect. Computer & System Engineering
University of Oviedo
Gijón, 33204, Spain
fernando@isa.uniovi.es

***Abstract*—Magnet demagnetization in permanent magnet synchronous machines (PMSMs) can lead to a reduction of the machine torque output and to an increase of the torque ripple, motor vibration and acoustic noise. Permanent magnet (PM) demagnetization detection is therefore a highly appealing feature. Local and global demagnetization patterns can be distinguished, the latter being the most likely to occur; both patterns can be uniform or non-uniform. Non-uniform global demagnetization of the PMs typically occurs due to a combination of high current and high PM temperature. This paper proposes the use of a search coil (SC) to detect and quantify non-uniform global demagnetization faults in interior PMSMs (IPMSMs). Magnitude and phase of the fundamental harmonic component of the SC flux linkage will be used with this purpose. Three different IPMSMs (integer slot, fractional slot, and concentrated winding IPMSMs) will be used to prove the validity of the proposed method.[1]**

Keywords—search coil, global non-uniform demagnetization, flux linkage, temperature

I. Introduction

Permanent magnet synchronous machines (PMSMs) have received significant attention over the last years due to their higher power and torque densities, efficiency and controllability compared with other types of electric machines. The performance of a PMSM directly depends on the magnetization state (MS) of the permanent magnets (PMs) as they are responsible for the main torque production capability in most PMSMs. PM demagnetization in PMSMs typically occurs due to a combination of excessive temperatures [1] and a high stator current, *d*- and/or *q*-axis [2], [3]. This is illustrated in Fig. 1: P_1 represents the PM operating point at no load and room temperature (T_1) condition. Then, if high load current is injected, the operating point of the PM is displaced to the left side of the BH curve, P_2, which is still located in the linear operating region of the BH curve. Thus, if the stator current is released, the PM operating point will return back to P_1, i.e., the PM has not been demagnetized. However, if the PM temperature is increased to T_2, the BH curve will shrink, the no load operating point of the PM being displaced from P_1 to P_3 (the PM flux density being reduced). If high stator current is injected at high temperature, PM operating point will be displaced from P_3 to e.g., P_4, which is out of the linear operating region of the BH curve. Therefore, if the load current is removed, the PM operating point will not return to P_3, but it will follow a recoil line, P_5 being reached, consequently the PM's flux linkage at no load has been reduced, i.e., the PM has been demagnetized.

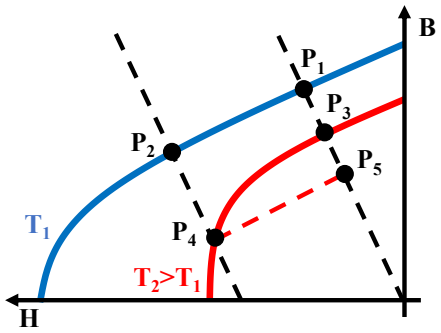

Fig. 1: PM operating point in BH curve for different load and temperature conditions.

Demagnetization can occur locally (i.e., differences in magnetization level among poles) or globally (i.e., same demagnetization pattern of all PMs), [4]. Moreover, global

[1] This work was supported in part by the Research, Technological, Development and Innovation Programs of the Spanish Ministry of Science and Innovation, under grant PID2019-106057RB-I00.

Table I: Comparative analysis of uniform global demagnetization detection methods

	Low cost	No additional hardware	Whole speed range	Insensitive to parameters
BEMF [17],[18]	✓	✓	×	✓
Pulse Injection [19]	✓	✓	✓	×
HFI [20],[21]	✓	✓	✓	×
SCs [14]-[16]	✓	×	×	✓
Hall-Effect [22]-[24]	×	×	✓	✓

demagnetization can be uniform (i.e., homogeneous MS within the PM) or non-uniform (i.e., non-homogeneous MS within the PM). Local demagnetization, e.g., due to hot spots, is less likely to occur, global demagnetization being more common during normal operation of the machine, e.g., due to temperature and/or stator current injection. Demagnetization will always result in a decrease of the average torque; in addition, non-uniform demagnetization produces an increase of the torque ripple, motor vibration and acoustic noise. PM demagnetization detection in PMSMs is therefore of great importance.

PMs' MS can be measured or estimated. PMs' MS can be measured by inserting a gauss meter in the machine air gap [4]; removing or drilling the end frame of the machine is required to insert the field sensor, field measurement being feasible only with the machine at standstill. Use of field sensors inserted between PMs and rotor lamination was proposed in [5]. Combined with a wireless transmission of the signal, this system provides online measurement of the MS and without interfering with the normal operation of the machine. Unfortunately, its cost is unacceptable for most applications, also it can compromise the robustness of the drive.

Alternatively to direct measurement, PMs' MS can be estimated. Local [6]-[16] and global [17]-[25] demagnetization detection/estimation methods have been already proposed. Table I summarizes the methods for uniform global demagnetization detection. BEMF based methods [17],[18], require the machine to be rotating. High frequency signal (HFI) and pulse injection-based methods [19]-[21] place concerns due to the adverse effects of the injected signal. Hall-effect sensors-based methods [22]-[24], require the installation of analog Hall-Effect sensors. Even if such sensors can be already present for control purposes, their characteristics and spatial location might not match with the requirements for PMs' MS estimation. Their installation places cost and robustness concerns. SCs [14]-[16] imply the installation of additional elements, also they require the machine to be rotating; nevertheless, they are a more cost-effective solution than Hall-effect based methods. Detection of non-uniform global demagnetization has received less attention, being only analysed for brushless DC machines (BLDC) in [25], the extension of this method to IPMSMs not being possible as it is based on the induced voltage at the non-excited phases.

Table II: Test machines' characteristics

Test Machine	1	2	3
Machine Type	IPMSM	VF-IPMSM	IPMSM
Phases (N_{ph})	3	3	3
Winding Type	ISW	FSW	CW
Stator slots (N_s)	36	60	9
Poles (P)	6	8	6
PMs Material	N42SH	N33SH / AlNiCo-9	N42SH
Rated Current	10A	11A	10A
Rated Speed	1000 rpm	3000 rpm	1000 rpm
Number of SCs	5	5	5

In this paper, a method for non-uniform global PMs' demagnetization detection and quantification in IPMSMs is proposed. The technique will be based on the variation of the fundamental harmonic component of the SC flux linkage. The proposed method will be validated throughout three IPMSM designs with different winding types and rotor designs.

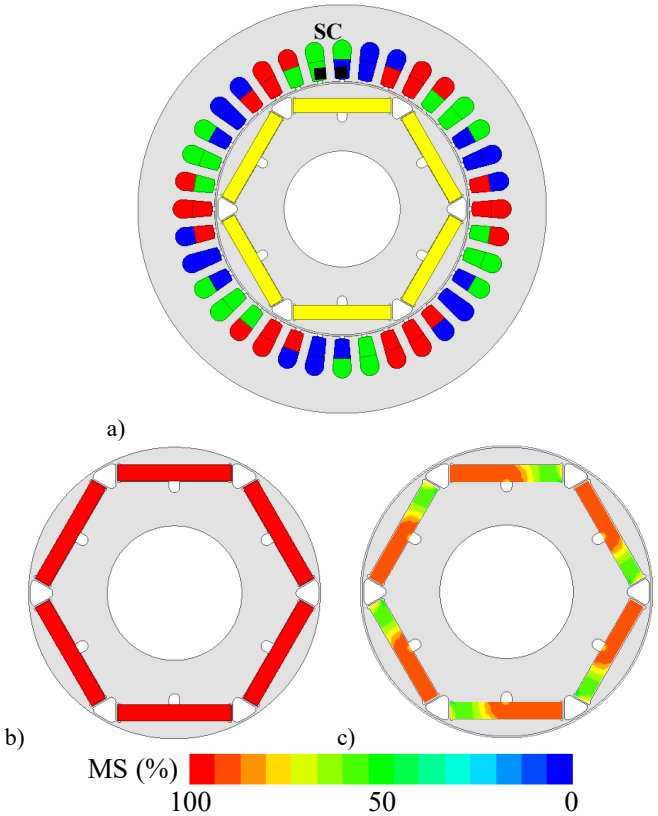

Fig. 2: a) 2D model of test machine 1, b) PMs' MS under healthy condition, **T = 20ºC**, and c) after injecting an overload current, **I_q = 75A, T = 180ºC.**

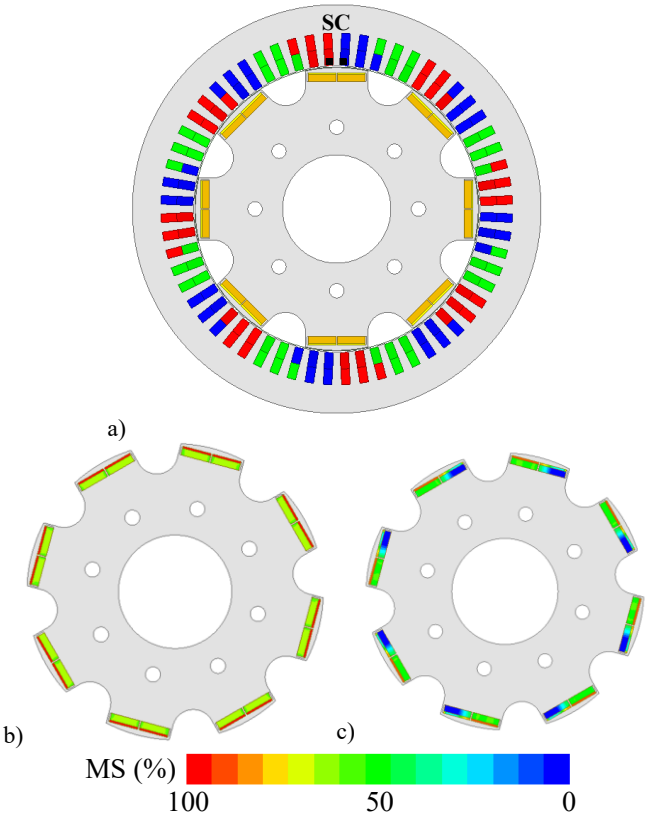

Fig. 3: Analogous results to Fig. 2 for test machine 2.

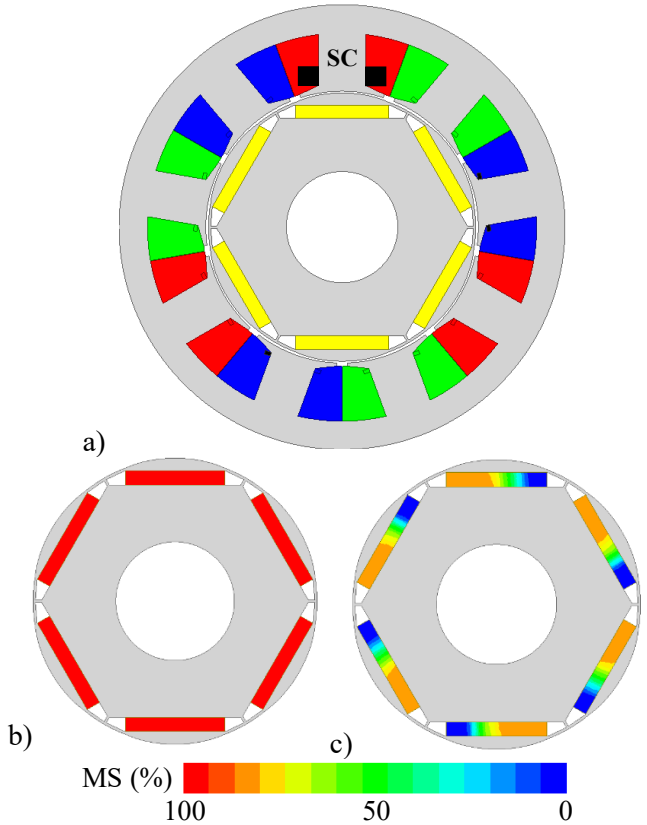

Fig. 4: Analogous results to Fig. 2 for test machine 3.

The paper is organized as follows: Section II analyses the effect of demagnetization due to load current and temperature in three different IPMSMs, and the detection possibilities through the SC flux linkage. Section III focuses on the implementation of the proposed method. Finite element simulation results verifying the effectiveness of the proposed detection and quantification techniques are included in Section IV. Conclusions are finally given in Section V.

II. PM Demagnetization Detection

This section provides simulation results of non-uniform global PM demagnetization in IPMSMs due to a combination of PM temperature and load current increase. First, the effect of the demagnetization fault on the PMs MS will be analysed. Then, its detection and quantification through the use of airgap SC measurements will be studied.

1) Effect of non-uniform global PM demagnetization on PMs MS

Three IPMSMs with different winding configurations and rotor designs will be used for this study, see Table II. Test machine 1 is an integer slot winding (ISW) IPMSM, i.e., $N_s/P/N_{ph}$ is integer. Test machine 2 is a fractional slot winding (FSW) IPMSM, i.e., $N_s/P/N_{ph}$ is non-integer and larger than 1. Test machine 3 is a concentrated winding (CW) IPMSM, i.e., $N_s/P/N_{ph}$ is fractional lower than 1. 2D models of these machines are shown in Figs. 2a, 3a and 4a, each machine being equipped with one SC wounded around one stator tooth. Fig. 2b, 3b and 4b show the MS of test machines under healthy condition at 20ºC, while Fig. 2c, 3c and 4c show the MS of test machines after overload load current injection at high temperature. Non-uniform global demagnetization pattern can be observed in the three machines, i.e., the trailing edge of the PMs is fully demagnetized. Note that there is a reduction in

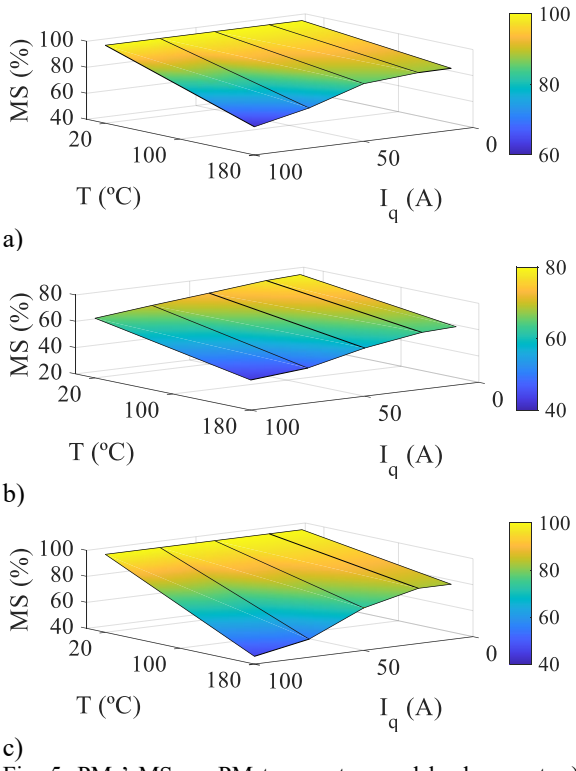

Fig. 5: PMs' MS vs. PM temperature and load current. a) test machine 1, b) test machine 2 and c) test machine 3.

the leading-edge MS, which is due to the PM flux decrease as temperature increases (see Fig. 1).

PM average MS can be used as a metric of PM demagnetization fault severity. Fig. 5a shows the global MS of test machine 1 depending on the amplitude of the load current and PMs temperature; it can be observed that MS always decreases almost linearly with temperature, large current levels increasing the MS vs. temperature slope. It is also observed that at ambient temperature, current has almost no effect on MS. Fig. 5b show analogous results to Fig. 5a for test machine 2. Conclusions for test machine 1 also apply in this case, the main difference being that at ambient

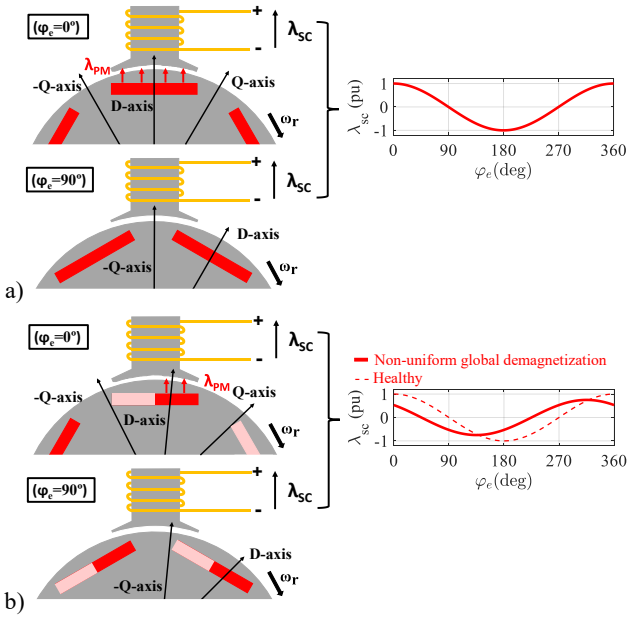

Fig. 6: Airgap SC flux linkage depending on the rotor position under a) healthy and b) global non-uniform demagnetization operation.

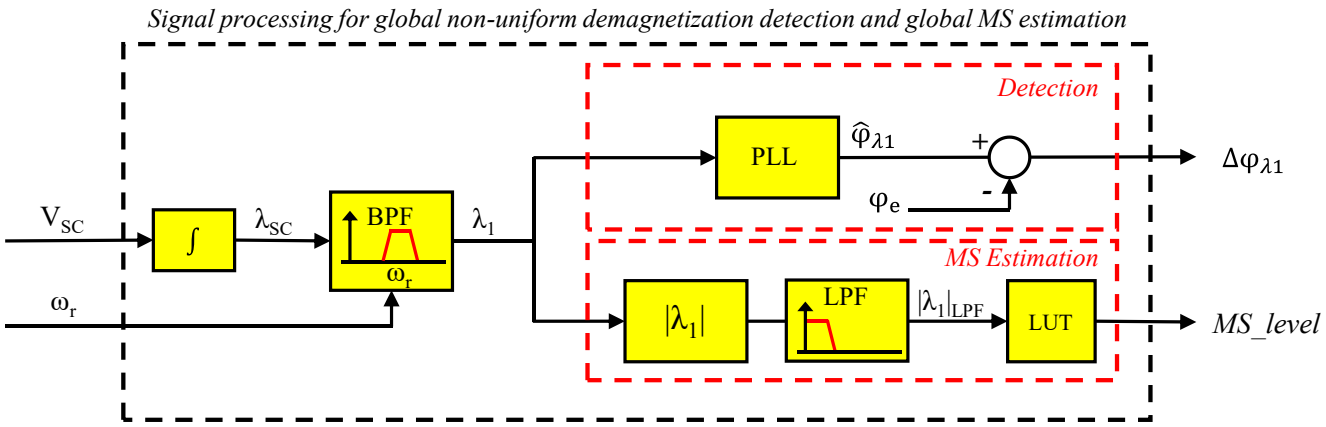

Fig. 7: Signal processing block diagram.

temperature, MS decreases with the current level due to the lower coercivity of AlNiCo-9 PMs (see Table II). Fig. 5c shows analogous results to Fig. 5a, the same conclusions hold.

2) Non-uniform global PM demagnetization on PMs MS using search coils

Fig. 6a shows the airgap flux ideally induced in a SC of a PMSM running in healthy operation vs. the rotor electrical angle, φ_e, a sinusoidal shape can be readily observed, its amplitude depending on the global MS of the PMs, p.u. has been used in this case for simplicity. If no stator current is injected, the airgap SC flux linkage will reach a maximum when a PM is located in front of the SC, i.e., the SC is aligned with the rotor *d*-axis, see Fig. 6a for φ_e=0º and 180º. In addition, zero-crossing occurs when the gap between two consecutive PMs is in front of the SC, i.e., the SC is 90 electrical degrees shifted from the *d*-axis, see Fig. 6a for φ_e =90º and 270º. Fig. 6b shows analogous results to Fig. 6a but when the machine has suffered a global, non-uniform demagnetization fault, note that the light red part of the PMs represents the region that has suffer demagnetization. It can be observed that the demagnetization fault leads to an unbalance between the MS of the leading and the trailing edge (the machine rotates in clockwise direction) of each PM (see Figs. 2-4c), which results in a displacement of the rotor *dq*-axes in the PMs' leading edge direction. As a result of this displacement, the airgap SC flux linkage suffers a phase shift (see the continuous red line in Fig. 6b) its amplitude also being reduced due to the global PMs' MS reduction, see Fig. 6b.

It can be concluded from the previous discussion that during a global, non-uniform demagnetization fault, the airgap flux linkage measured by a SC will suffer: i) a phase shift due to the displacement of the rotor *d*-axis, produced by the unbalanced MS of the PMs and ii) a decrease in its magnitude due to the reduction of the global MS of the PMs. Therefore, monitoring i) the phase angle, and ii) the magnitude of the fundamental component of the airgap flux linkage measured by the SC will allow to identify a global non-uniform demagnetization fault and estimate the global MS of the PMs.

III. Implementation

Fig. 7 shows the signal processing block diagram for the implementation of the proposed non-uniform global demagnetization detection method. Two different stages are distinguished:

Fault detection: it is done by monitoring the phase angle of λ_{sc} fundamental component. First, λ_{sc} is obtained by integrating the measured SC voltage, V_{sc}. Then, a band-pass filter (BPF), with center-frequency adaptive to the rotor rotational frequency, will be used to isolate the fundamental component of λ_{sc}, i.e., λ_1. After that, a PLL will be used to estimate the phase of λ_1, $\hat{\varphi}_{\lambda 1}$. Finally, the difference between $\hat{\varphi}_{\lambda 1}$ and the electrical rotor position, which is measured by an incremental encoder, φ_e, will be used to obtain λ_1 phase deviation, $\Delta\varphi_{\lambda 1}$, respect healthy operation.

Fault quantification: it is done by obtaining the rectified and low-pass filtered value of the fundamental component of λ_{sc}, $|\lambda_1|_{LPF}$. First, λ_1 (which is obtained during the fault detection process) is rectified, $|\lambda_1|$ being obtained. Then a 2Hz cut-off frequency low-pass filter is used to get the mean value

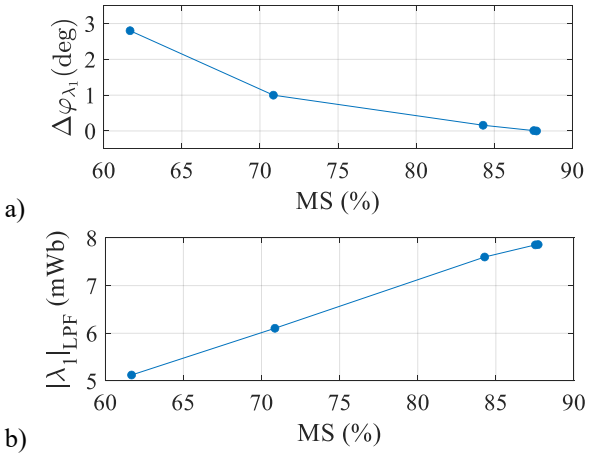

Fig. 8: a) $\Delta\varphi_{\lambda 1}$ and b) $|\lambda_1|_{LPF}$ vs MS of test machine 1. **T=180ºC**.

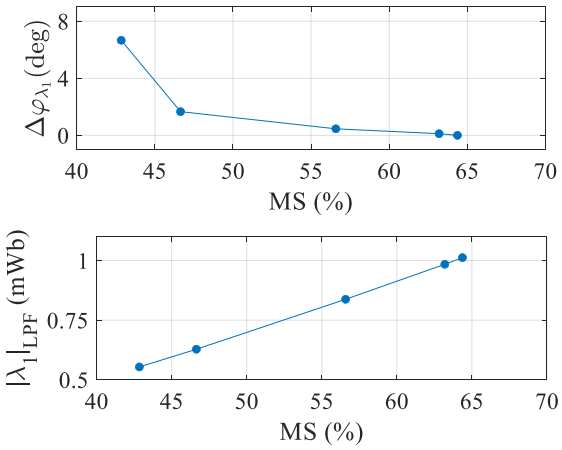

Fig. 9: Analogous results to Fig. 8 for test machine 2.

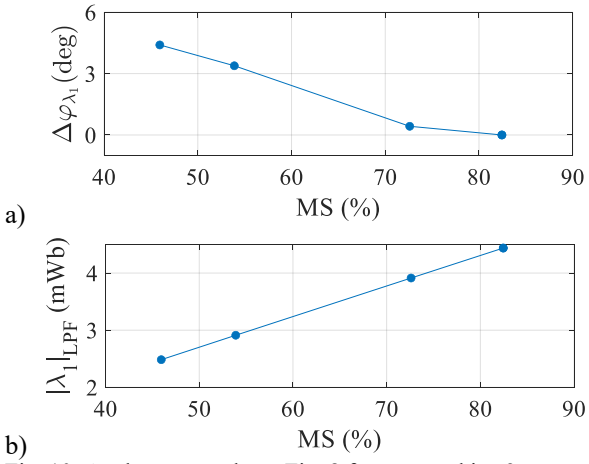

Fig. 10: Analogous results to Fig. 8 for test machine 3.

of $|\lambda_1|$, $|\lambda_1|_{LPF}$ being obtained, note that different cut-off frequencies can be selected depending on the machine design, operating condition, application, etc. Finally, a look-up table will be used to obtain the MS estimation signal, MS_level.

IV. Simulation Results

This section shows simulation results using the proposed global non-uniform demagnetization detection and quantification technique.

Fig. 8a and b show $\Delta\varphi_{\lambda 1}$ vs. the PMs MS and $|\lambda_1|_{LPF}$ vs. PMs MS for test machine 1; $\Delta\varphi_{\lambda 1}$ is seen to follow an exponential behavior with MS while $|\lambda_1|_{LPF}$ decreases linearly with the PMs MS. It can be concluded that $\Delta\varphi_{\lambda 1}$ can be used as a metric to detect and assess the depth of a global non-uniform demagnetization fault, while $|\lambda_1|_{LPF}$ can be used to estimate the global MS of the PMs. Figs. 9 and 10 show analogous results to Fig. 8 for test machines 2 and 3, the same conclusions that for test machine 1 hold for these machines.

Fig. 11 shows FE simulation results using the proposed global, non-uniform demagnetization detection and quantification method, see Fig. 7, for test machine 1, a *q*-axis current pulse has been used to produce the non-uniform demagnetization fault at high temperature. Fig. 11a shows the *dq*-axes currents, note that the time axis has been zoomed to appreciate the injected *q*-axis current pulse (t=1s). Fig. 11b shows the PMs' MS before and after the current injection, a global non-uniform demagnetization profile can be readily observed after the pulse injection. Fig. 11c shows V_{sc} before and after load current injection, Fig. 11d shows λ_{sc}, which is estimated by integrating V_{sc}, see Fig. 11c. Fig. 11e shows $\Delta\varphi_{\lambda 1}$ (see Fig. 7), an increase from 0 to ≈1 electrical degree can be observed, i.e., the global, non-uniform demagnetization fault can be detected from this variation. Fig. 11f shows $|\lambda_1|_{LPF}$ (see Fig. 7), its amplitude is seen to decrease after the current pulse due to the PMs' global MS decrease. Finally, a LUT is used to get MS_level from $|\lambda_1|_{LPF}$, see Fig. 11g, quantification of the global MS of the PMs being therefore achieved.

Figs. 12 and 13 show analogous results to Fig. 11 for test machines 2 and 3, the same conclusions as for test machine 1 can be reached.

From the previous discussion, it can be concluded that both $\Delta\varphi_{\lambda 1}$ and $|\lambda_1|_{LPF}$ can be used as reliable metrics for global non-uniform demagnetization detection and MS estimation, respectively.

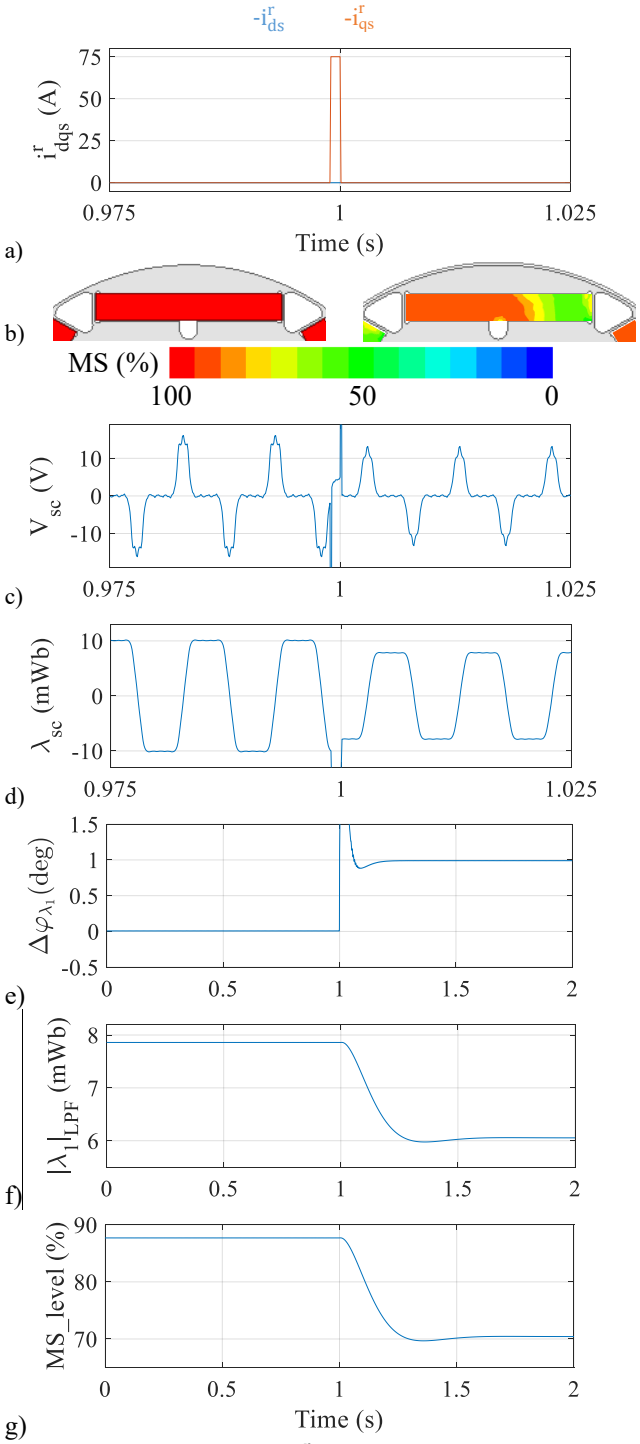

Fig. 11: a) *dq*-axes currents, i^r_{dqs}, b) PMs' MS profile, c) SC voltage, V_{SC}, d) SC flux linkage, λ_{SC}, e) $\Delta\varphi_{\lambda 1}$, f) $|\lambda_1|_{LPF}$ and g) MS_level before and after a demagnetization current pulse for test machine 1. **I_q=75A, T=180ºC.**

V. Conclusions

The combination of high rotor temperature and load current injection can lead to irreversible demagnetization in the trailing edge of the PMs of a PMSM. Simulation results have been provided to verify this phenomenon. This paper proposes the use of the fundamental component of the SC flux linkage, λ_1, to detect and quantify non-uniform global demagnetization faults in IPMSMs. Three IPMSMs with different winding configurations (ISW, FSW and CW) and rotor designs have been used to prove the validity of the proposed method. It has been shown that global non-uniform

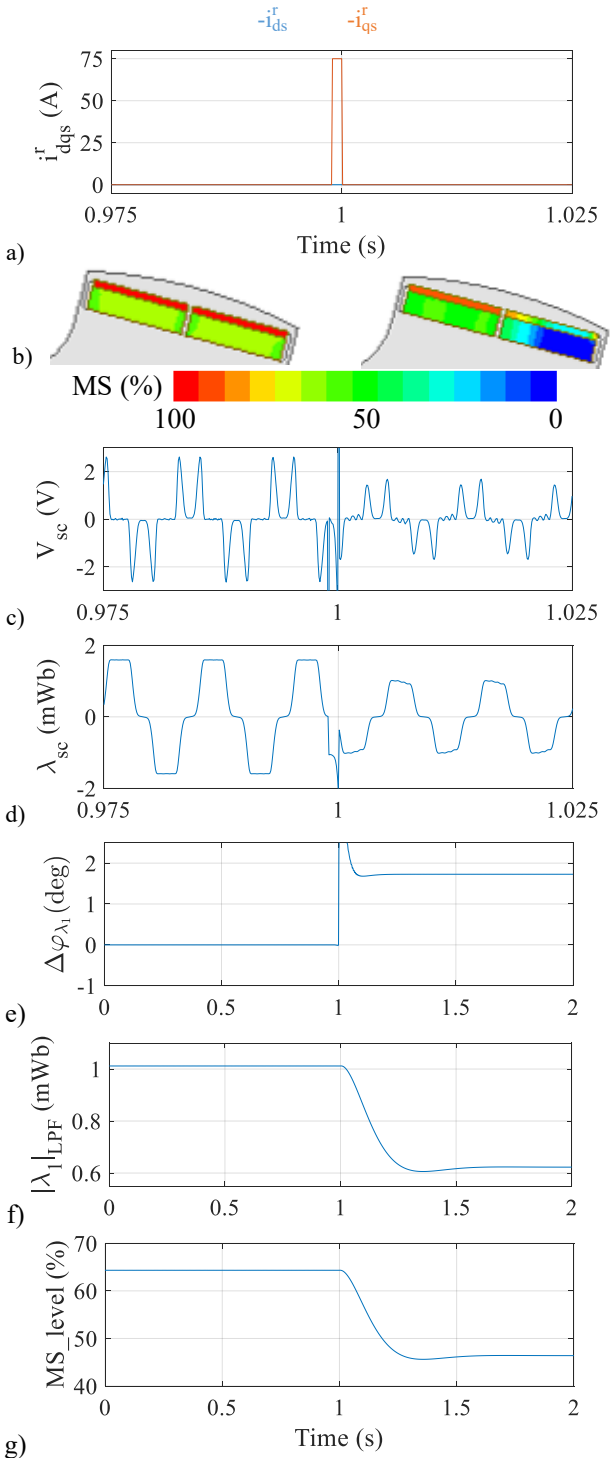

Fig. 12: Analogous results to Fig. 11 for test machine 2.

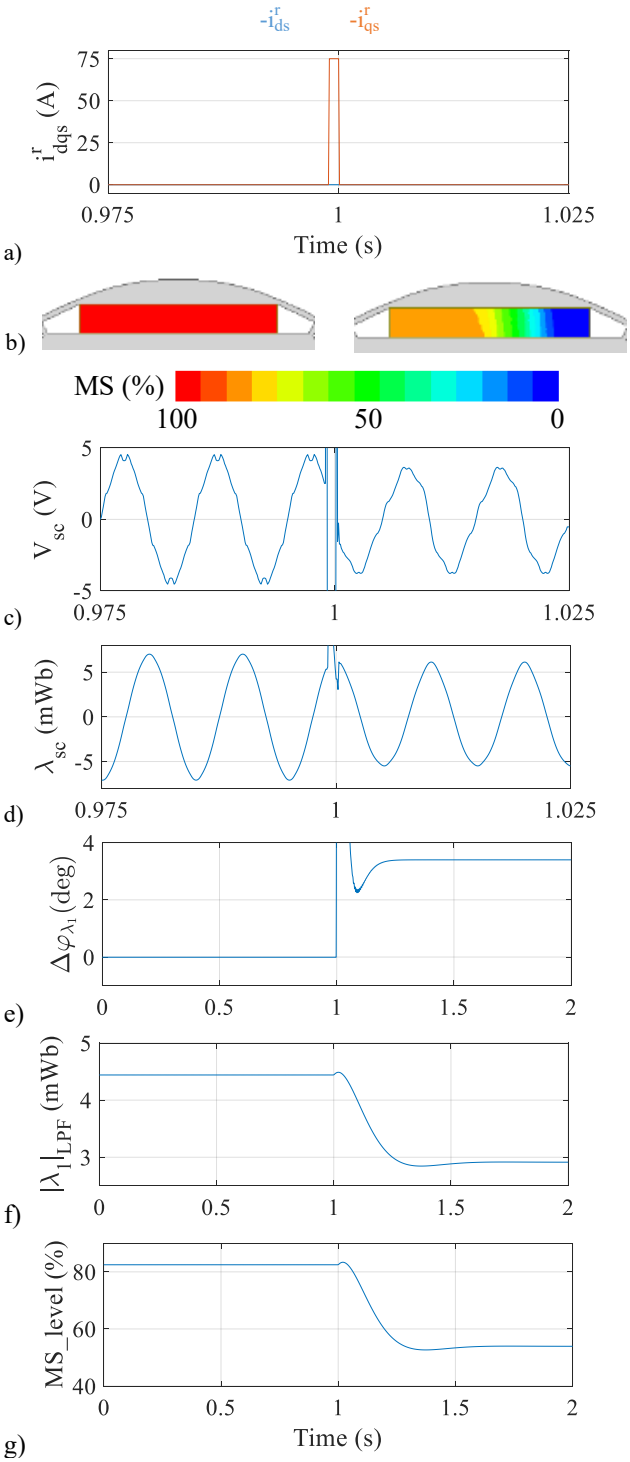

Fig. 13: Analogous results to Fig. 11 for test machine 3.

demagnetization faults lead to displacements in the phase of λ_1, while reducing its magnitude; both variables can be used therefore as metrics to detect and quantify non-uniform global demagnetization faults. Signal processing for implementing the proposed methods has been provided. Finite element simulation results have been used to verify the effectiveness of the proposed methods for the three test machines.

REFERENCES

[1] D. Reigosa, D. Fernandez, H. Yoshida, T. Kato, and F. Briz, "Permanent magnet temperature estimation in PMSMs using pulsating high-frequency current injection," IEEE Trans. Ind. Appl., vol. 51, no. 4, pp. 3159–3168, Jul./Aug. 2015.

[2] N. Limsuwan, T. Kato, K. Akatsu, and R. D. Lorenz, "Design and evaluation of a variable-flux flux-intensifying interior permanent-magnet machine," IEEE Trans. Ind. Appl., vol. 50, no. 2, pp. 1015–1024, Mar./Apr. 2014.

[3] S. Ruoho, J. Kolehmainen, J. Ikaheimo and A. Arkkio, "Interdependence of Demagnetization, Loading, and Temperature Rise in a Permanent-Magnet Synchronous Motor," IEEE Trans. Magn., vol. 46, no. 3, pp. 949–953, Mar. 2010.

[4] J Hong, D Hyun, and S.B.Lee, "Automated monitoring of magnet synchronous motors at standstill," IEEE Trans. Ind. Appl., 46 (4): 1397 -1405, 2010.IEC 62. 2-2004., "IEEE guide for diagnostic field testing of electric power apparatus-electrical machinery," 2004.

[5] D. Fernandez, D. Reigosa, T. Tanimoto, T. Kato, and F. Briz, "Wireless permanent magnet temperature & field distribution

measurement system for IPMSMs," IEEE ECCE, pp. 3996–4003, Sep. 2015.
[6] J.-R. R. Ruiz, A. G. Espinosa, L. Romeral, and J. Cusidó, "Demagnetization diagnosis in permanent magnet synchronous motors under non- stationary speed conditions," Electr. Power Syst. Res., 80(10): 1277–1285, Oct. 2010.
[7] S. Rajagopalan, W. le Roux, T. G. Habetler, and R. G. Harley, "Dynamic eccentricity and demagnetized rotor magnet detection in trapezoidal flux (brushless DC) motors operating under different load conditions," IEEE Trans. Power Electron., 22(5): 2061–2069, Sep. 2007.
[8] C. Urresty, J.-R. R. Ruiz, M. Delgado, and L. Romeral, "Detection of demagnetization faults in surface-mounted permanent magnet synchro- nous motors by means of the zero-sequence voltage component," IEEE Trans. Energy Convers., 27(1): 42–51, Mar. 2012.
[9] J. C. Urresty, J.-R. R. Ruiz, and L. Romeral, "A back-EMF based method to detect magnet failures in PMSMs," IEEE Trans. Magn., 49(1): 591–598, Jan. 2013.
[10] Z. Yang, X. Shi, and M. Krishnamurthy, "Vibration monitoring of PM synchronous machine with partial demagnetization and inter-turn short circuit faults," in Proc. IEEE ITEC, pp. 1–6, June 2014.
[11] D. Torregrossa, A. Khoobroo and B Fahimi, "Prediction of Acoustic Noise and Torque Pulsation in PM Synchronous Machines With Static Eccentricity and Partial Demagnetization Using Field Reconstruction Method", IEEE Trans. on Ind. Elect., 59(2): 934–944, Feb. 2012.
[12] J. C. Urresty, R. Atashkhooei, J.-R. R. Ruiz, L. Romeral, and S. Royo, "Shaft trajectory analysis in a partially demagnetized permanent-magnet synchronous motor," IEEE Trans. Ind. Electron., 60(8): 3454–3461, Aug. 2013.
[13] J. Hong, D. Hyun, S.B. Lee, J.Y. Yoo and K.W. Lee, "Automated Monitoring of Magnet Quality for Permanent-Magnet Synchronous Motors at Standstill," IEEE Trans. Ind. Appl., 46(4): 1397–1405, July-Aug. 2010.
[14] M. S. S. Rafaq et al., "Airgap Search Coil based Identification of PM Synchronous Motor Defects," in IEEE Transactions on Industrial Electronics, doi: 10.1109/TIE.2021.3095810.
[15] Y. Da, X. Shi and M. Krishnamurthy, "A New Approach to Fault Diagnostics for Permanent Magnet Synchronous Machines Using Electromagnetic Signature Analysis," in IEEE Transactions on Power Electronics, vol. 28, no. 8, pp. 4104-4112, Aug. 2013, doi:10.1109/TPEL.2012.2227808.
[16] M. O. Zapico, D. D. Reigosa, H. J. Lee, M. S. Rafaq, S. B. Lee and F. B. del Blanco, "Demagnetization Detection in PMSMs Using Search Coils Exploiting Machine's Symmetry," 2021 IEEE Energy Conversion Congress and Exposition (ECCE), 2021, pp. 4460-4467, doi: 10.1109/ECCE47101.2021.9595756
[17] X. Xiao, C. Chen and M. Zhang," Dynamic Permanent Magnet Flux Estimation of Permanent Magnet Synchronous Machines", IEEE Trans. on Appl. Sup., 20(3): 1085–1088, June. 2010.
[18] K. Liu and Z. Q. Zhu "Online Estimation of the Rotor Flux Linkage and Voltage-Source Inverter Nonlinearity in Permanent Magnet Synchronous Machine Drives," IEEE Trans. on Pow. Elect., 29(1): 418-427, Jan. 2014.
[19] K. Liu, Q. Zhang, J. Chen, Z. Q. Zhu, and J. Zhang, "Online multiparameter estimation of nonsalient-pole PM synchronous machines with temperature variation," IEEE Trans. Ind. Electron., vol. 58, no. 5, pp. 1776–1788, May 2011.
[20] D. Reigosa, D. Fernandez, J. M. Guerrero, Z.Q. Zhu and F. Briz, "PMSM Magnetization State Estimation Based on Stator-reflected PM Resistance Using High Frequency Signal Injection", IEEE Trans. on Ind. Appl., 51(5): 3800-3810, Sept.-Oct. 2015.
[21] D. Fernandez, D. Reigosa, Z.Q. Zhu and F. Briz, "Permanent-Magnet Magnetization State Estimation Using High-Frequency Signal Injection", IEEE Trans. on Ind. Appl., 52(4): 2930-2949, July-Aug. 2016.
[22] D. Reigosa et al., "Detection of Demagnetization in Permanent Magnet Synchronous Machines Using Hall-Effect Sensors," in IEEE Transactions on Industry Applications, vol. 54, no. 4, pp. 3338-3349, July-Aug. 2018, doi: 10.1109/TIA.2018.2810123.
[23] Y. Park et al., "Online Detection and Classification of Rotor and Load Defects in PMSMs Based on Hall Sensor Measurements," in IEEE Transactions on Industry Applications, vol. 55, no. 4, pp. 3803-3812, July-Aug. 2019, doi: 10.1109/TIA.2019.2911252.
[24] Y. Park et al., "Online Detection of Rotor Eccentricity and Demagnetization Faults in PMSMs Based on Hall-Effect Field Sensor Measurements," in IEEE Transactions on Industry Applications, vol. 55, no. 3, pp. 2499-2509, May-June 2019, doi: 10.1109/TIA.2018.2886772.
[25] D.-H. Kim, J. H. Im, U. Zia, J. Hur, "Online detection of irreversible demagnetization fault with non-excited phase voltage in brushless dc motor drive system," Proc. of IEEE ECCE, pp. 748-753, 2020.